The Kinetics of Inactivation of the Rod Phototransduction Cascade with Constant Ca^{2+}_i

A. LYUBARSKY,* S. NIKONOV,*‡ and E. N. PUGH, JR.*

From the *Department of Psychology and Institute of Neurological Sciences, University of Pennsylvania, Philadelphia, Pennsylvania 19104-6196; and the ‡Institute of Cellular Biophysics, Academy of Sciences, Puschino, Russia

ABSTRACT A rich variety of mechanisms govern the inactivation of the rod phototransduction cascade. These include rhodopsin phosphorylation and subsequent binding of arrestin; modulation of rhodopsin kinase by S-modulin (recoverin); regulation of G-protein and phosphodiesterase inactivation by GTPase-activating factors; and modulation of guanylyl cyclase by a high-affinity Ca^{2+}-binding protein. The dependence of several of the inactivation mechanisms on Ca^{2+}_i makes it difficult to assess the contributions of these mechanisms to the recovery kinetics in situ, where Ca^{2+}_i is dynamically modulated during the photoresponse.

We recorded the circulating currents of salamander rods, the inner segments of which are held in suction electrodes in Ringer's solution. We characterized the response kinetics to flashes under two conditions: when the outer segments are in Ringer's solution, and when they are in low-Ca^{2+} choline solutions, which we show clamp Ca^{2+}_i very near its resting level. At T = 20–22°C, the recovery phases of responses to saturating flashes producing $10^{2.5}$–$10^{4.5}$ photoisomerizations under both conditions are characterized by a dominant time constant, $\tau_c = 2.4 \pm 0.4$ s, the value of which is not dependent on the solution bathing the outer segment and therefore not dependent on Ca^{2+}_i. We extended a successful model of activation by incorporating into it a first-order inactivation of R*, and a first-order, simultaneous inactivation of G-protein (G*) and phosphodiesterase (PDE*). We demonstrated that the inactivation kinetics of families of responses obtained with Ca^{2+}_i clamped to rest are well characterized by this model, having one of the two inactivation time constants (τ_{R^*} or τ_{PDE^*}) equal to τ_c, and the other time constant equal to 0.4 ± 0.06 s.

INTRODUCTION

The biochemical events underlying the activation of the phototransduction cascade in vertebrate rods and cones are now well established (Pugh and Lamb, 1993; Hofmann and Heck, 1995). Moreover, recent investigations have also shown that models of activation based on the established biochemical events of phototransduction can provide quantitatively accurate accounts of the amplification and kinetics of the electrical responses of vertebrate rods (Lamb and Pugh, 1992; Pugh and Lamb, 1993; Kraft et al., 1993), and of the α-wave of the human electroretinogram (Breton et al., 1994; Hood and Birch, 1994), which is proportional to the activation phase of the rod photocurrent (Hagins et al., 1970).

Address correspondence to Dr. E. N. Pugh, Jr., Department of Psychology, University of Pennsylvania, 3815 Walnut Street, Philadelphia, PA 19104-6196.

The biochemical processes governing the inactivation of the phototransduction cascade and the recovery phase of the photoresponse are less well understood than those governing activation, although a number of mechanisms have been discovered and characterized in vitro that down-regulate, or otherwise modulate each of the activation steps. The enzymatic activity of photoactivated rhodopsin (R*) has been shown to be diminished by phosphorylation by rhodopsin-kinase (RK), and by the subsequent binding of the 48-kD protein arrestin (Sitaramayya and Liebman, 1983; Wilden et al., 1986; Bennett and Sitaramayya, 1988). Moreover, the activity of RK is modulated in a Ca^{2+}-dependent manner by S-modulin (alias recoverin) (Kawamura, 1993; Chen et al., 1995; Klenchin et al., 1995). The inactivation of the activated moiety of G-protein, $G_{t\alpha}$-GTP, and of its target protein, the rod phosphodiesterase (PDE), are apparently coupled via the GTPase activating effect of PDE_γ, the inhibitory subunit of the PDE (Arshavsky and Bownds, 1992). Other GTPase activating factors may

also be involved (Angleson and Wensel, 1994). In addition, the inactivation rate of the PDE–$G_{t\alpha}$–GTP complex may depend on the occupancy of cGMP on noncatalytic binding sites on PDE_α and PDE_β (Arshavsky et al., 1992, 1994). Guanylyl cyclase (GC) activity is regulated by a high-affinity, multisite calcium binding protein, GCAP (Gorczya et al., 1994; Palczweski et al., 1994), in such a way that the decline in $Ca^{2+}{}_i$ that occurs during the light response increases GC activity and accelerates the recovery of the circulating current after a flash of light (Hodgkin and Nunn, 1988; Fain et al., 1989; Nakatani and Yau, 1989).

Efforts to link the recovery kinetics of the photoresponse with the biochemistry of inactivation of the photoreceptor cascade in situ must confront a number of problems. One problem is that the different biochemical inactivation processes occur concurrently in the responses of intact photoreceptors, making it difficult to analyze the contributions of individual processes to the overall kinetics. Another problem is that dynamic changes in $Ca^{2+}{}_i$ accompany normal photoresponses, and, as noted above, such changes modulate several of the biochemical events hypothesized to underlie response recovery.

In an effort to confront these problems and link the kinetics of photoresponse recovery in intact amphibian rods more quantitatively to the underlying biochemistry, in the investigation presented here we used three strategies. First, we adapted the experimental approach of Fain et al. (1989) and Nakatani and Yau (1989), blocking the action of the Na^+/Ca^{2+}-K^+ exchanger and eliminating Ca^{2+} influx, thus freezing $Ca^{2+}{}_i$; this approach allows the recovery kinetics to be characterized without the complexity of dynamically changing $Ca^{2+}{}_i$. Second, we extended a previous representation of the activation of the phototransduction cascade (Lamb and Pugh, 1992) by incorporating first-order inactivation of the two enzymatic amplifiers, R* and PDE*, and we have characterized the recovery kinetics in constant $Ca^{2+}{}_i$ in terms of two corresponding theoretical time constants, τ_{R^*} and τ_{PDE^*}. Third, we adopted and extended the analysis of David Pepperberg and colleagues, who have provided evidence that a characteristic time parameter, τ_c, derived from the photoresponse recovery kinetics, corresponds to a time constant, τ_{R^*}, of first-order decay of the enzymatic activity of R* (Pepperberg et al., 1988, 1992; Kahlert et al., 1990). Our results allow us to examine the dependence of τ_c on $Ca^{2+}{}_i$.

The paper is organized as follows. First, in the Theory section we develop a phototransduction cascade model that incorporates inactivation steps and that is appropriate for describing responses in the choline solution. Second, we present the Methods. Third, we present data (in Figs. 3–7) characterizing the experimental protocol used to clamp $Ca^{2+}{}_i$ to its resting value and evaluate its success in doing so. Fourth, we measure τ_c, the dominant time constant of photoresponse recovery in normal Ringer's solution and in calcium-clamping conditions (Figs. 8 and 9) and analyze the results by applying the model (Figs. 10 and 11, and Table I). Finally, we discuss the implications for the understanding of the mechanisms of inactivation of the transduction cascade.

THEORY

The theoretical description of the phototransduction cascade of salamander rods applied here has for the most part been presented in previous papers (Cobbs and Pugh, 1987; Hodgkin and Nunn, 1988; Lamb and Pugh, 1992; Pugh and Lamb, 1993). However, to incorporate a biochemical description of the recovery phase of the photoresponses, we have extended our previous formulation, which dealt almost exclusively with the activation phase (Lamb and Pugh, 1992). Moreover, to characterize the inverted photoresponses obtained in choline solution, we have found it necessary to introduce some theoretical considerations not treated in previous papers. Thus, we present here an abbreviated description of the extended model.

Major Steps in the Phototransduction Cascade

The model divides the activation events of the cascade into five major steps. The first three take place at the disc membrane and can be characterized by the following chemical scheme:

$$R \rightarrow R^* \overset{\tau_{R^*}}{\rightarrow} R_{\text{inactive}} \tag{1}$$

$$G_{\alpha\beta\gamma} \overset{\nu_{RG}}{\curvearrowright} G_\alpha{}^* \tag{2}$$

$$+$$

$$PDE \rightarrow G_\alpha{}^* \cdot PDE^* \overset{\tau_{PDE^*}}{\rightarrow} G_{\text{inactive}}, PDE_{\text{inactive}} \tag{3}$$

Step 1 is the generation of the active enzyme R* by the photoisomerization of rhodopsin and its subsequent conversion to metarhodopsin II. Step 2 is the catalytic production by R* at the rate ν_{RG} of G*, the active moiety of G-protein; the arched arrow signifies catalysis. Step 3 is the stoichiometric activation of catalytic subunits of PDE by G*. Lamb and Pugh (1992) showed that in the absence of inactivation, the numbers of the activated proteins *R**, *G**, and *PDE** produced in an outer segment in response to a flash producing Φ photoisomerizations could be well described as these functions of time: a step (*R**), a ramp (*G**), and a delayed ramp (*PDE**), respectively, with the amplitude of the

TABLE I

Variables and Parameters of the Cascade Model

Variables	Interpretation	Range/value (unit)
Φ	Number of photoisomerizations per flash	
$R^*(t)$	Number of activated rhodopsins at time t	0–3.5×10^9
$G^*(t)$	Number of free, activated G-proteins at time t	0–$3.5 \times 10^8 = G_{tot}$
$PDE^*(t)$	Number of activated PDE catalytic subunits	0–$2.6 \times 10^7 = PDE_{tot}$
$cG(t)$	The concentration of free cGMP in the outer segment	$<<K_{1/2}$ for channel
$F_c(t)$	Normalized circulating current in choline at time t	0–1
Parameters	**Interpretation**	**Value/status**
ν_{RG}	Rate of production of G* by single R*	Estimated ($= A/c_{GP}\beta_{sub}n$)
ν_{RP}	Rate of production of PDE* per R*	Estimated ($= A/\beta_{sub}n$)
c_{GP}	Coupling efficiency factor between G* and PDE*	0.8
τ_{R^*}	Time constant for inactivation of R* catalytic activity	Estimated as τ_c
τ_{PDE^*}	Time constant for inactivation of G*-PDE*	Estimated by curve fitting
$\alpha(t)$	Rate of synthesis of cGMP by GC	$\approx\alpha_{dark}$ (see Eq. 11)
α_{dark}	Dark rate of cGMP synthesis	2.4 $\mu M\ s^{-1}$ ($= \beta_{dark}cG_{dark}$)
β_{sub}	Rate constant of cGMP hydrolysis by single PDE catalytic subunit in a volume equal to that of the outer segment cytoplasm	$1.9 \times 10^{-5}\ s^{-1}$
$\beta(t)$	Rate constant of PDE activity in outer segment	$\equiv PDE^*(t)\ \beta_{sub} + \beta_{dark}$
β_{dark}	Rate constant of cGMP hydrolysis in the dark	$0.6\ s^{-1}$
cG_{dark}	Resting cytoplasmic concentration of cGMP	4 μM
n	Hill coefficient of the cGMP-activated channels in situ	2.5
A	Amplification constant; equal to $\nu_{RG}\ c_{GP}\beta_{sub}n$	Estimated
ρ	Ratio of slope conductances: g'_{is}/g'_{cG} (Eq. 11; cf. Fig.1)	2.3

The formulation and symbols are those adopted by Lamb and Pugh (1992) and Pugh and Lamb (1993); the calculations are done for an isotropic rod outer segment; whereas this is an oversimplification, it can be computationally justified under certain conditions (Lamb and Pugh, 1992). The value of β_{sub} in this table reflects recent advances in the characterization of the kinetic parameters of amphibian rod PDE (Dumke et al., 1994). The value of β_{dark} is taken from the investigation of Hodgkin and Nunn (1988); they give $b_n = n\beta_{dark} = 1.54 \pm 0.36\ s^{-1}$ (17 rods); thus for $n = 2.5$, we obtained $\beta_{dark} = 0.6$. We emphasize that over the intensity range used in these experiments the numerical values of τ_{R^*} and τ_{PDE^*} can be interchanged without affecting the model's behavior (Eq. 4; Discussion). Estimated = the parameter value was estimated from application of the model to data of individual rods.

step and the slopes of the ramps proportional to Φ. Further theoretical analysis supporting this conclusion can be found in Lamb (1994). The scheme shown in steps 1–3 extends this model by incorporating a first-order inactivation of R* and a simultaneous first-order inactivation of G* and PDE*.

The hypothesis expressed in step 1, that the enzymatic activity of R* decays as a first-order exponential, might seem unreasonable in view of the complexity of mechanisms that down-regulate R* (Introduction); nonetheless, it is an extant and tractable hypothesis (Pepperberg et al., 1992). Steps 2 and 3 embody the hypothesis that G* and PDE* are inactivated by one and the same molecular event, most likely the hydrolysis of the terminal phosphate of G* = $G_{t\alpha}$-GTP when it is complexed with a PDE_γ (Arshavsky and Bownds, 1992; Introduction). This coupling is effected by allowing G* to decay only when it is bound to a PDE catalytic subunit.

For salamander rods, which have discs with surface areas of $\sim$100 μm^2 per side, it can be expected that the reaction scheme 1–3 will be linear in intensity for flashes producing up to 10 or more R*'s per disc face, or $\sim$20,000 total photoisomerizations (Lamb and Pugh, 1992; Lamb, 1994). For such intensities $PDE^*(t)$, the number of active phosphodiesterase catalytic subunits in the outer segment at time t after a flash can be predicted to obey approximately the following equation:

$$PDE^*(t) = \Phi\nu_{RP}\ C\left(e^{-t/\tau_{R^*}} - e^{-t/\tau_{PDE^*}}\right). \qquad (4)$$

Here Φ is the number of photoisomerizations produced by the flash ν_{RP}, is the rate of production of PDE^*'s per fully active R*, τ_{R^*} and τ_{PDE^*} are time constants for the inactivation of R* and PDE* as seen in the scheme 1–3, and $C = (\tau_{R^*}\tau_{PDE^*})/(\tau_{R^*} - \tau_{PDE^*})$ is a constant. The rate ν_{RP} of production of PDE^*s is related to the rate of production of G^*s in step 2 by $\nu_{RP} = \nu_{RG}\ c_{GP}$, where c_{GP} is a coupling coefficient that is expected to be close to unity (Lamb and Pugh, 1992; Lamb, 1994). At early times when the exponentials in Eq. 4 could be approximated by the first terms in their Tay-

lor series, Eq. 4 reduced to $PDE^*(t) = \Phi \nu_{RP} t$, which is the ramping result of Lamb and Pugh (1992). Eq. 4 neglects the brief delay in activation that has been examined previously (Lamb and Pugh, 1992); this delay is of little consequence on the relatively long time scales examined here. The delay can be introduced into Eq. 4 by replacing t with $t' = t - t_{eff}$, with $t_{eff} \approx 15$–20 ms, and by setting $PDE^*(t') = 0$, $t' \leq 0$. This was done in the computational implementation.

Whereas the local depletions of the unactivated forms of G-protein and PDE that occur at the disc surface during activation are implicitly incorporated into the activation parameters ν_{RG} and ν_{RP}, the global depletions of these unactivated forms that are expected to occur at sufficiently high intensities are neglected. This neglect is because the intensities used in these experiments should not cause such depletions (see below, Computational Implementation of the Model).

The fourth major step of the cascade is the regulation of the concentration of free cGMP, cG, by the two enzymes, PDE and GC. In an isotropic rod outer segment this rate equation governs cG, the concentration of free cGMP:

$$\frac{dcG}{dt} = \alpha - \beta cG \ . \tag{5}$$

In Eq. 5, α is the rate of synthesis of cGMP by GC and depends on a number of factors, including (and especially) Ca^{2+}_i; β is the rate constant of cGMP hydrolysis by phosphodiesterase, which is generally time- and light-dependent, and dependent on the buffering power of cGMP.

The final major step in the cascade is the relationship between cG and the recorded circulating current. In previous formulations, this relationship has been expressed succinctly in terms of F, the fraction of circulating current present at any instant:

$$\begin{aligned} F(t) &\equiv \frac{J(t)}{J_{dark}} \\ &= \left(\frac{cG(t)}{cG_{dark}}\right)^n. \end{aligned} \tag{6}$$

In Eq. 6, cG_{dark} is the concentration of cGMP in darkness (at rest), $J(t)$ is the (light-sensitive) circulating current measured at any instant in time in a particular solution, J_{dark} is the magnitude of J in darkness, and n is the Hill coefficient of the cGMP-activated conductance.

Five established principles underlie the use of Eq. 6 to characterize the responses of non–voltage-clamped rods in Ringer's solution. First, the current/voltage relation of the cGMP-activated current in normal Ringer's solution has a very shallow slope in the normal operating voltage range of the rod (Baylor and Nunn, 1986). Second, the cGMP-activated current equilibrates within milliseconds with free cGMP (Cobbs and Pugh, 1987; Karpen et al., 1988). Third, the voltage dependence and cGMP dependence of the cGMP-activated channels are assumed to be independent of one another, i.e., to act as separable functions (Baylor and Nunn, 1986). Fourth, capacity currents and electrogenic exchange currents are generally negligible with respect to the circulating current (see Cobbs and Pugh, 1987; Lamb and Pugh, 1992). Fifth, $cG << K_{1/2}$, the half-saturation point of the Hill relation for the current through the channels (Yau and Baylor, 1989). Although all five principles involve approximations, in normal Ringer's solution the approximations are very good, and Eq. 6 provides a faithful representation of the cGMP-activated current over the normal voltage range of the rod.

Eq. 6 will not apply under conditions in which the relevant region of the current/voltage relation of cGMP-activated current has a significant slope, as it does in a choline solution containing almost no permeant cations. Fig. 1 serves to illustrate why Eq. 6 is inappropriate and also helps to explain the alternative relationship we have adopted. Unlike the situation in normal Ringer's solution (Fig. 1 *A*), in a choline solution lacking permeant cations the cGMP-activated current is outward (Fig. 1 *B*) and has a significant slope conductance, violating one of the principles underlying Eq. 6. To develop an appropriate alternative to Eq. 6, we begin with the assumption that under the recording conditions

$$J_{is} = -J_{cG}. \tag{7}$$

Here, J_{is} is the inner segment component of the circulating current, and J_{cG} is the outer segment, cGMP-activated component (Fig. 1 *B*). Eq. 7, like Eq. 6, assumes electrogenic exchange and capacity currents to be negligible. The problem with using Eq. 7 to derive an alternative to Eq. 6 is that in choline solution, both sides of Eq. 7 depend on the membrane potential, as illustrated in Fig. 1 *B*. To deal with this complication, we approximated the current/voltage relations of the inner segment current and of the cGMP-activated current by linear relations over the range of voltage excursion that the membrane potential undergoes during a saturating light response in choline solution:

$$\begin{aligned} J_{cG} &= g'_{cG}\left(\frac{cG}{cG_{dark}}\right)^n (V - V_{cG}), && V_{cG} < V \leq V_{is}; \\ &= 0, && V \leq V_{cG}; \end{aligned} \tag{8}$$

$$J_{is} = (V - V_{is}), \qquad V_{cG} \leq V \leq V_{is} \ . \tag{9}$$

In Eqs. 8 and 9, V is the membrane potential, V_{cG}, the reversal potential of the cGMP-activated conductance in choline solution, V_{is} the reversal potential of the in-

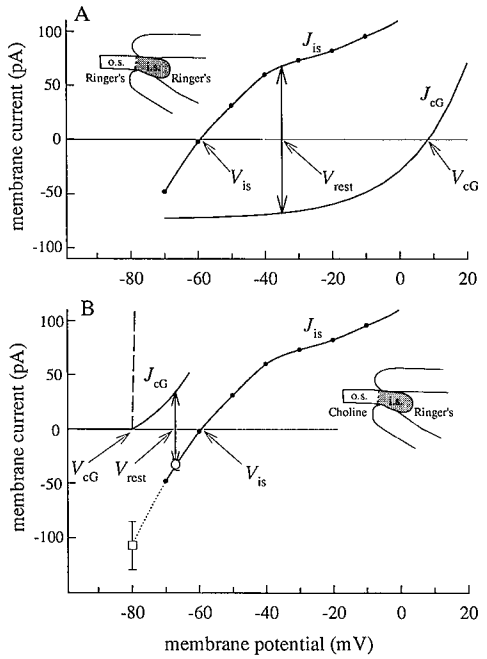

FIGURE 1. Current/voltage curves for the inner segment and outer segment components of the circulating current of a model salamander rod, the inner segment of which is held in an ideal suction pipette in normal Ringer's solution, and the outer segment of which is either in Ringer's solution, or in 0-Ca^{2+} choline solution (see *inset*, Fig. 3 for the actual configuration of a rod in the suction pipette). (*A*) Outer segment in normal Ringer's solution. J_{cG} identifies the cGMP-activated current of the outer segment in Ringer's solution, and follows the current/voltage relation of Baylor and Nunn (1986). The asymptotic magnitude of J_{cG} at hyperpolarized voltages is assumed to be 73 pA, based on the salamander rod whole-cell data of Cobbs and Pugh (1987) and Miller and Korenbrot (1994). J_{is} is the steady state inner segment current/voltage curve of Bader et al. (1979); the filled circles plot their actual measurements, through which a smooth curve has been interpolated. The resting membrane potential of the model rod in Ringer's solution is $V_{rest} = -35$ mV; this is the potential when J_{cG} and J_{is} are in balance, i.e., equal in magnitude and opposite in sign. V_{cG} and V_{is} identify the membrane potentials at which the curves J_{cG} and J_{is} intersect the 0-current axis. During a light response the membrane potential is driven from V_{rest} toward V_{is} as the cGMP-activated current declines. (*B*) Outer segment in 0-Ca^{2+} choline solution. When the outer segment is jumped into a choline solution containing no permeant cations, J_{cG} (*unbroken curve*) shifts to the left of the inner segment current curve J_{is}. The inner segment component of the circulating current J_{is} nonetheless follows the same current/voltage relation as in *A*, since the inner segment remains in Ringer's solution inside the suction pipette. Thus, the potential V_{rest} at which J_{is} and J_{cG} are in balance is now hyperpolarized with respect to V_{is}, and the circulating current reverses its direction of flow (e.g., as seen in the data of Fig. 3). The values of V_{rest} and V_{cG} were estimated as follows. The two open symbols with error bars represent circulating current magnitudes measured in 0-Ca^{2+}-choline under two conditions: at rest (○) and when cG is raised to a high level (□). These two data points are placed on the graph so that they lie on the J_{is} curve, which has been extrapolated with a polynomial approximation (*dotted curve*). At rest, J_{cG} (*unbroken curve*) must pass through a value equal in magnitude and opposite in sign to the point ○; this condition determines the value V_{rest}. When cG is raised to a high level, J_{cG} (*dashed curve*) becomes much steeper than at rest, the overall circulating current is limited by J_{is}, and V_{is} driven arbitrarily close to V_{cG}. Thus, V_{cG} is identified as the potential corresponding to the lower data point (□). During a light response in choline, as cGMP declines from its resting value the membrane potential will depolarize from V_{rest} toward V_{is}, and thus the maximal voltage excursion is expected to be ~10 mV. The magnitudes of the data points (○, □) were obtained from suction electrode measurements made in 0-Ca^{2+} choline and are reported in connection with Fig. 5; they assume a suction electrode collection efficiency of two thirds (the error bars are ±1 SD). The curves J_{cG} in *B* were generated with the same form of current/voltage relation as used by Baylor and Nunn (1986), but are completely outwardly rectified, reflecting the absence of permeant cations in the choline solution. In the model developed in the text, J_{cG} and J_{is} are approximated by straight lines (Eqs. 8 and 9, respectively) over the potential range between V_{cG} and V_{is}, and for cG at and below its resting value cG_{dark}.

ner segment current, and g'_{cG} and g'_{is} the respective slope conductances. Eq. 8 implicitly employs two of the general principles used in obtaining Eq. 6, viz., that the voltage dependence and cGMP dependence of the cGMP-activated channels are separable, and that $cG << K_{1/2}$, the half-saturation concentration for current activation. In the experimental design used here, the inner segment is always held in a suction electrode in normal Ringer's solution; thus Eq. 9 is simply a linear approximation of the normal inner segment current/voltage relation in the relevant, relatively small voltage domain (see Fig. 1 *B*). Eqs. 7–9 can be solved for V, and by substitution of the resultant expression for V into Eq. 8 and algebraic manipulation, the following expression can be obtained relating F_C, the normalized circulating current of a rod whose outer segment is in a choline solution with negligible permeant cations, to outer segment cG:

$$F_c \equiv \frac{J_{cG}}{(J_{cG})_{dark}} = (1 + \rho)\left[\frac{\left(\frac{cG}{cG_{dark}}\right)^n}{\left(\frac{cG}{cG_{dark}}\right)^n + \rho}\right]. \quad (10)$$

Here $\rho = g'_{is}/g'_{cG}$, the ratio of the slope conductances of the overall inner segment conductance and the cGMP-activated conductance, in the neighborhood of the membrane potential at rest ($cG = cG_{dark}$) in choline. Based on results we report below (see Fig. 5), we estimate the value of ρ to lie between 1.5 and 3 for individual rods. We note that Eq. 10 reduces to Eq. 6 as $\rho \to \infty$, which is the condition that holds at rest in Ringer's solution, in which the slope conductance of the cGMP

current is nearly zero (Baylor and Nunn, 1986). It also bears mention that Eq. 10 is not dependent on the specific values of $V_{rest,C}$ and V_{is}.

In sum, the assumptions underlying Eq. 10 are reasonable and consistent with established facts. Moreover, whereas Eq. 10 is more complex than Eq. 6, it differs principally in having a saturating relation between cG and F_C even when $cG << K_{1/2}$. Finally, as we will show, when combined with Eq. 4, Eq. 10 allows extension of the cascade theory to the full time course of families of responses of rods whose outer segments are in a choline solution with negligible amounts of permeant cations.

Computational Implementation of the Model

For intensities that do not lead to global depletion of the unactivated forms of G-protein and PDE, Eq. 4 is expected to be an accurate representation of $PDE^*(t)$, the number of photoactivated PDE catalytic subunits generated by the chemical scheme 1–3. For the values of the parameters involved (Tables I and II) and the intensities used in the experiments reported here, such depletion can be shown to be negligible to modest. For example, for $A = 0.06\ s^{-2}$, $n = 2.5$, $\beta_{sub} = 1.9 \times 10^{-5}$, one can derive from Table I the estimates $\nu_{RP} = 1{,}260\ s^{-1}$, and $\nu_{RG} = 1{,}580\ s^{-1}$. For $\tau_{R^*} = 2.4$ s and $\tau_{PDE^*} = 0.4$ s, according to Eq. 4 the peak production of PDE* will occur at < 2 s, and so for $\Phi = 2 \times 10^4$, $PDE^*(t) \leq \Phi\nu_{RP} \times 2 = 2.5 \times 10^7$, a value less than the total complement of PDE catalytic subunits. If τ_{R^*} is lower, significant depletion of the inactive form of PDE will occur at still higher intensities. Since there is more than 10 times as much G-protein as PDE, significant depletion of unactivated G-protein will not occur until much higher intensities.

Eq. 5 was solved with the fourth–fifth order Runge-Kutta routine ODE45 of MatLab. The time-varying forcing factor $\beta(t)$ was computed as $\beta(t) = \beta_{dark} + PDE^*(t)\beta_{sub}$, where β_{dark} and β_{sub} are given in Table I. The term α was also allowed to be time dependent, as expressed in Eq. 12; the rate parameter k_α was estimated from application of Eq. 5 to the DC–LC trace (e.g., lowermost trace in Fig. 7).

The normalized circulating current in choline, $F_C(t)$, was computed with Eq. 10, with $\rho = 2.3$, the value estimated from the results reported in the context of Fig. 5. For computational convenience it was assumed that $cG = cG_{dark}$ at $t = 5$ s after the jump to choline.

An equation for capacity current was also added to provide a good account of the activation phase of responses to bright flashes. This addition can be made without knowledge of the absolute values of V, providing a membrane time constant can be assumed, and the cell impedance does not change during the activation phase of the response. Based on the work of a number of laboratories on salamander rods, we expect τ_m to be ~20 ms. Cobbs and Pugh (1987) showed how τ_m can be estimated from the responses to bright flashes.

METHODS

Some of the methods used in this investigation have been reported previously (Cobbs and Pugh, 1987). The description presented here emphasizes those experimental procedures and analyses that are novel or especially important for this report.

Animals and Tissue Preparation

Larval tiger salamanders (*Ambystoma tigrinum*) were obtained from Charles Sullivan (Nashville, TN) and maintained in aerated, charcoal-filtered tanks on a diet of minnows. Retinas were prepared and rods isolated, as described previously.

Solutions

All solutions were made with tissue-culture–grade water (W3500, Sigma Chemical Co., St. Louis, MO) and reagent-grade chemicals. The contents of the normal amphibian Ringer's solution in millimolars were: NaCl, 111; KCl, 2; $CaCl_2$, 1.0; Na_2HPO_4, 0.5; $MgCl_2$, 1; $MgSO_4$, 0.5; EDTA, 0.01; HEPES, 3. The pH was adjusted with NaOH to 7.4. We also added 2 mg/ml fatty-acid–free bovine serum albumin (A6003, Sigma Chemical Co.) to the Ringer's solution; this seemed particularly helpful in keeping cells viable immediately after the chopping, when debris from ruptured cells is present.

In preliminary experiments aimed at maintaining constant Ca^{2+}_i in rods, we used several different 0-Na^+/low-Ca^{2+} external solutions, including solutions containing either guanidinium (Nakatani and Yau, 1989; Fain et al., 1989) or K^+ or Mg^{2+} as the only cation; each of these conditions provided some useful data. However, we found that the 0-Na^+ solution that yielded stable recordings for the longest periods was a choline solution (Hodgkin et al., 1984; Matthews, 1995), the constituents of which were (in mM): choline–chloride, 115; HEPES, 3; glucose, 10; and small amounts of Ca^{2+}, buffered with 2 mM EGTA (L657-5, Baker); we emphasize that no Mg^{2+} or any other permeant cation was added. The pH of choline solutions was adjusted by adding of small amounts of tetramethylammonium. The osmolarity of the choline solutions was measured with a vapor pressure osmometer (model 5500, Westcor Inc., Logan, UT), and matched empirically to that of the Ringer's solution with small adjustments of the choline–chloride concentration; this adjustment helped maintain long-term stability of rods.

Estimation of Free Calcium in the Choline Solutions

Methods for calculating free Ca^{2+} in physiologic solutions buffered with EGTA have been examined by Durham (1983) and Tsien (1983). In the absence of Mg^{2+}, the four stability constants involved are those for the binding of the first and second protons to $EGTA^{4-}$, that for the binding of Ca^{2+} to $EGTA^{4-}$, and that for the binding of Ca^{2+} to EGTA-H^{3-}, respectively. Based on

Durham's (1983) survey and an analysis of the literature, we adopted the following values for these constants at 20°C: pK_{H1} = 9.5, pK_{H2} = 8.94, pK_{Ca} = 11.38, and pK_{CaH} = 5.7. A program was written in MatLab that iteratively solved the set of simultaneous binding equations involved and that checked for conservation of the EGTA and calcium. Experimentally, we used only five levels of $Ca^{2+}{}_o$ with choline. Specified in terms of (free Ca^{2+} | total Ca^{2+}) the first four levels were (7.4 nM | 900 μM); (6.1 nM | 800 μM); (2.3 nM | 400 μM); and (1.0 nM | 200 μM). The fifth level, 0-Ca^{2+} choline, refers to solutions with 2 (or, rarely, 10) mM EGTA and no added Ca^{2+}. We emphasize that other than the very small amounts of Ca^{2+} *no* permeant cations were added to the choline solutions.

Recording Chamber and Solution Exchange

All experiments were performed at room temperature (20–22°C) under continuous infrared illumination ($\lambda \geq 850$ nm) in a light-tight Faraday cage built over an inverted microscope (IM-35, Carl Zeiss, Inc., Thornwood, NJ) on a vibration-isolation table. Fig. 2 illustrates the experimental chamber and superfusion system, which was modeled on previously reported superfusion chambers for photoreceptors (Hodgkin et al., 1985, 1987; Lamb and Matthews, 1988). The top (*1*) and bottom (*2*) of the chamber are 1-mm-thick glass slides, mounted on Plexiglas blocks (*3, 4*). The sides of the chamber are open to permit entry of electrodes from both sides. The chamber dimensions are 8 × 3 × 1.4 mm, and its volume is 33 μl.

In the experiments, two solutions continually flowed into the chamber under gravity feed: the main flow was through the body of the block (*inlet 1*) and usually carried Ringer's solution; the secondary flow, which usually carried choline test solutions, was through a central polycarbonate tube (*5, inlet 2*), having an outside diameter of 600 μm, and an inside diameter of 300 μm. A six-way tap allowed selection of additional solutions for the secondary flow. The solution exit was through a channel in the body of block 4 and was connected to a small open bath in which fluid was maintained at a constant level by continous suction through a small tube. A Ag/AgCl reference electrode was connected to the bath by means of a short salt bridge with a wick; the electrode was connected to the signal ground of the recording amplifier. Gravitational gradients and flow resistance were adjusted to give flow rates of 0.5–1.0 ml min^{-1} for the main flow, and 0.05–0.1 ml min^{-1} for the test flow. Control experiments with dye in the central flow showed that with these rates the flows are laminar, with sharp boundaries extending from the tube orifice up to 1 mm beyond the end of the tube. The flow rates were chosen to be as low as possible to prevent bending of the rods, yet able to produce good laminar boundaries.

For electrical recording, the inner segment of a salamander red rod was drawn into a tapered suction pipette filled with normal Ringer's solution. The resistance of the suction electrode without a rod inserted was 0.5–0.6 MΩ and with the rod in place increased to 2–3 MΩ. Each rod was carefully positioned in the pipette so that the inner segment/outer segment junction was just *outside* the point of maximal pipette constriction (see Fig. 2 *B* and Fig. 3, *left inset*); this was done to ensure that the entire outer segment was exposed to the choline superfusion solution. Previous experiments combining suction electrode recordings and whole-cell recordings showed that when a rod is optimally placed in the tapered type of suction electrode that we construct, approximately two thirds of the circulating current is recovered by the suction electrode (Cobbs and Pugh, 1987). Because of the positioning of the rods, the suction electrode collection should be between one half and two thirds.

Once the rod was properly seated in the suction pipette, the chamber and pipette were arranged so that the rod occupied a standard position 180–200 μm from the center of the superfusion tube in an *x–y* plane containing the tube's central axis (Fig. 2 *B*). Recording then commenced. Changes in the solution superfusing the rod were effected by a computer-controlled motormike (Oriel Corporation of America, Stamford, CT) which was mounted rigidly on the stage of the microscope and which translated the chamber along the *x* coordinate. The forward movement of the chamber situated the rod on the superfusion tube's central axis, < 100 μm from the orifice; the reverse movement caused the chamber to return to its original position, so that the rod was again in the main flow. The speed of the solution change was estimated from the kinetics of the junction current recorded with a rod exposed to a bright light; 90% of the junction current occurred in 200–300 ms (see Fig. 3).

Light Stimulation and Intensity Calibrations

Rods were stimulated with circularly polarized 500-nm light from a multibeam optical system constructed on the vibration table and situated outside the Faraday cage (Cobbs and Pugh, 1987). One channel of the stimulator could deliver flashes (usually 10 ms in duration) or steps of any duration. The other channel delivered 20-μs flashes. Both stimulus channels contained optical wedges that were under the control of a microcomputer, allowing 0.02 log unit steps in intensity over > 3 log units of intensity. Additional neutral density filters were available in each of the channels. A dedicated microcomputer having customized software controlled the timing of the light stimuli and their synchronization with the stage movements.

Light intensities were calibrated regularly at the microscope stage with a Pin-10 photodiode (United Detector Technology) that had been calibrated absolutely by the National Research Council of Canada. Intensities were expressed in flux density units (quanta μm^{-2} s^{-1} or quanta μm^{-2} $flash^{-1}$) at the image plane of the microscope. The optical wedges and neutral filters were recalibrated for these experiments. For simplicity in reporting the results, we assume that a salamander red rod has a collecting area of 18 μm^2 for the circularly polarized, 500-nm stimuli used here (see Lamb and Pugh, 1992). This collecting area reflects the use of a 500-nm rather than a 520-nm stimulus (the λ_{max} of salamander porphyropsin), and a 20-degree tilt of the rod with respect to the horizontal plane. In the text below, stimuli are expressed in photoisomerizations, Φ or Φ s^{-1}, obtained by multiplying the quantal flux density at the stage by the assumed collecting area. No corrections have been applied for loss of light caused by scattering in the chamber.

Electrical Recording and Data Analysis

A patch-clamp amplifier (model 8900, Dagan Corp., Minneapolis, MN) with a 1-GΩ head stage having 10-kHz bandwidth served as the current-to-voltage transducer for measuring the membrane current of the rod inner segment. The output of the Dagan amplifier was fed to a four-pole analogue Bessel filter (model

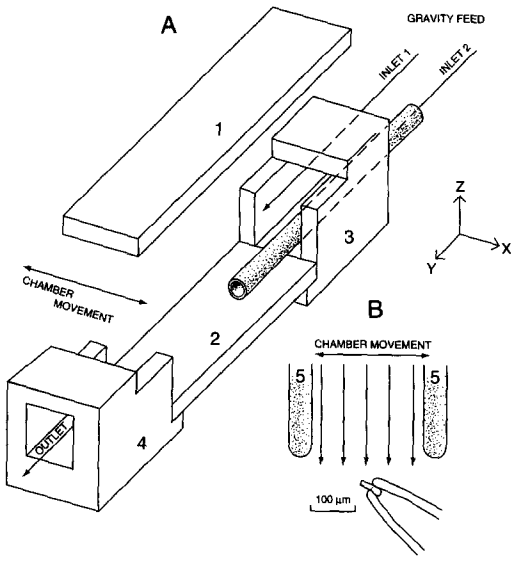

FIGURE 2. (*A*) Schematic of the experimental chamber. Two glass plates (*1* and *2*) are mounted on Plexiglas blocks (*3* and *4*). Solutions flow into the chamber either through the main block (*inlet 1*) or through the central tube (*inlet 2*, stippled); laminar flows are maintained by gravity feed from small wells attached to the input side of the chamber. (*B*) Disposition of a rod in a suction pipette when exposed to the test solution in the central tube (drawing is approximately to scale).

3323, Krohn-Hite Corp., Avon, MA) and then to a 12-bit A/D converter (TL1-1, Axon Instruments, Foster City, CA) interfaced with a microcomputer (486/33, Gateway) that used software that enabled it to serve as an oscillographic display during the experiments and store the digitized records on magnetic disk and tapes for off-line processing (Axotape, Axon Instruments, Foster City, CA). For most of the experiments the sampling rate was set to 100 Hz, although for a number of experiments sampling rates up to and including 500 Hz were used. The corner frequency of the analogue filter was set at a value appropriate to avoid aliasing, e.g., at 200 Hz for 500-Hz sampling. Stimulus markers were recorded on one of several parallel data channels.

Continuous digitized records were divided into appropriate time blocks based on the stimulus markers and analyzed with customized software constructed on the MatLab platform. The software allowed for averaging records, subtracting baselines, response normalization, curve fitting, and other routine analysis procedures.

RESULTS

Fig. 3 illustrates the basic experimental protocol used throughout this paper and serves further to illustrate a number of features of the method. The experiment was patterned on that of Fain et al. (1989; Fig. 4) and was designed to maintain Ca^{2+}_i constant at the level it has in the dark, resting state. Shown are suction electrode traces obtained from a rod whose outer segment was exposed repeatedly to 0-Ca^{2+} choline solution. For 10 of the traces the rod was stimulated with each of a series of increasingly intense flashes in Ringer's solution, and then again after 5 s in choline solution, with the same flash; a saturating flash was then given to determine the residual circulating current in choline solution, and the rod was returned to the Ringer's solution. For the two traces marked *LC* (light control), the rod was stimulated with a saturating flash before being moved to choline; for the trace marked *DC* (dark control), only a single flash was given in choline, at the time when the second flash was normally delivered.

Of critical importance for the kinetic analyses that we undertake here is that the rod remain stable for a long recording period. For the rod of Fig. 3, the superfusion cycle Ringer's → choline → Ringer's was executed more than 90 times, allowing repeated responses to each flash to be obtained. During the nearly 3 h of recording, the circulating current and light response kinetics in Ringer's solution were maintained with only modest change. In general we found that rods having initial photocurrents under these recording conditions of 35–50 pA (Table II) were stable for dozens of solution changes and for recording periods of 2 h or more.

Experiments Examining the Stability of Ca^{2+}_i in Low-Ca^{2+} Choline Solution

Since most previous experiments in which investigators have attempted to maintain Ca^{2+}_i constant in rods have employed guanidinium or lithium as the charge carrier of cGMP-activated current, it is important to examine the evidence for stability of Ca^{2+}_i in choline solution. Some pertinent evidence is presented in Fig. 3 in the inset showing the difference trace, *DC–LC*. This difference trace reveals that the light-sensitive current increased steadily at a rate of 0.5 pA s^{-1} during the 15-s exposure to the low-Ca^{2+} choline solution. Assuming that β_{dark}, the rate constant of cGMP hydrolysis in darkness, remains constant during the choline exposure, the steady increase in circulating current necessitates a steady increase in α, the rate of cGMP synthesis (Eq. 5). Because the most likely cause of the increase in α is a steady decline of Ca^{2+}_i, a careful examination is required of the suitability of the 0-Ca^{2+} choline condition for maintaining Ca^{2+}_i near its resting level.

To test the hypothesis that a decline of Ca^{2+}_i underlies the steady increase in circulating current and to assess the rate and magnitude of changes in Ca^{2+}_i, we performed experiments designed to vary Ca^{2+}_i over its natural range in normal Ringer's solution, and to establish the maximum circulating current achievable in 0-Ca^{2+} choline solution.

Fig. 4 *A* shows data obtained from a rod repeatedly jumped into 0-Ca^{2+} choline solution in darkness. In this experiment, to clearly delineate any changes in circulating current, a saturating flash was delivered at a series of different times after the jump. These data confirm the inference drawn from the *DC–LC* trace in Fig.

3, viz., the circulating current steadily increases in 0-Ca^{2+} choline. They also yield the additional observation that the rate of increase declines over 30 s. The finding that the rate of increase declines was replicated on several rods (see Fig. 6 *C*). In the experiments reported here, we never kept a rod in choline longer than 30 s.

Fig. 4 *B* shows results from the same rod, but in each case exposed before the switch to choline to a step of light that suppressed about two thirds of the circulating current in Ringer's solution. An increase in circulating current in choline over the level seen in Fig. 4 *A* was expected, because the light step in Ringer's solution lowers Ca^{2+}_i, thereby increasing GC activity and leading to elevated *cG* once PDE activity has declined to its dark level (see Eq. 5). The maximum circulating current in choline in Fig. 4 *B* was 53 pA, 2.4-fold greater than the circulating current recorded at the same point in time without prior light exposure (Fig. 4 *A*). The maximum magnitude of the circulating current seen in Fig. 4 *B* provides a quantitative perspective on the rate of increase of current in the dark shown in Fig. 4 *A*, for it shows the magnitude of the rate, 0.5 pA s^{-1}, to be relatively small. Moreover, 53 pA represents a lower bound on the maximum possible current in 0-Ca^{2+} choline solution, since partial suppression of the circulating current in Ringer's solution does not cause Ca^{2+}_i to decline to its lowest possible value, nor does it cause GC to achieve its maximum rate (Hodgkin and Nunn, 1988). We now describe additional experiments designed specifically to estimate the maximal possible current achieveable in 0-Ca^{2+} choline.

To estimate the maximum circulating current achieveable in 0-Ca^{2+} choline, we performed experiments similar to that of Fig. 4 *B* but varied the intensity of the light steps in Ringer's solution; such experiments are similar to the experiments performed by Fain et al. (1989) to evaluate calcium clamping in solutions having guanidinium as the charge carrier through the cGMP-activated channels. We also performed experiments in which we jumped rods into 0-Ca^{2+} choline containing 50–500 μM IBMX, with and without prior light adaptation. These maneuvers are expected to increase *cG*, both by further increasing GC activity before the jump into choline and by decreasing PDE activity after the jump (Hodgkin and Nunn, 1988). Fig. 5 presents results from three such experiments. In each panel the trace labeled *D* is the circulating current observed when the jump into 0-Ca^{2+} choline solution was made in darkness and without IBMX; the other traces are circulating currents obtained when the cell was exposed before the jump to a step of light that suppressed at least 50% of its current (*L*) or obtained when IBMX was added to the choline solution (*I*). For seven rods exposed to various combinations of light steps and IBMX, the maximum circulating current in 0-Ca^{2+} choline solution was 71 ± 15 pA (mean ± SD). The value 71 pA provides an estimate of the circulating current achieved when the cGMP conductance is very strongly activated in 0-Ca^{2+} choline, and the membrane potential approaches V_{cG} (see Fig. 1 *B*); let us call this value J_{max}. For these same seven rods, the circulating current measured in darkness at 5 s after the jump was 22 ± 5 pA; call this value J_{dark}. (In Fig. 1 *B*, J_{max} and J_{dark}, corrected from suction electrode collection efficiency, are plotted as the two open symbols.) The ratio J_{max}/J_{dark} is

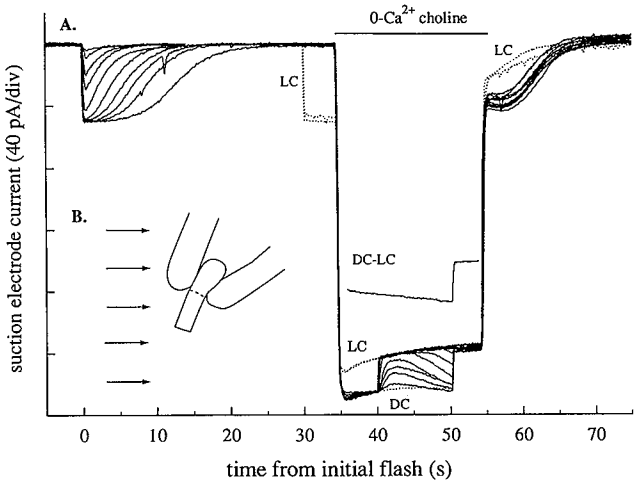

FIGURE 3. (*A*) Suction electrode records for a rod repeatedly exposed to 0-Ca^{2+} choline. In 10 of the cycles shown the rod was stimulated at $t = 0$ with a flash of preset intensity, and then, after the switch to choline at $t = 40$ s, the same flash was repeated. At $t = 50$ s, a saturating flash was delivered to determine any residual circulating current, and at $t = 54$ s, the cell was returned to Ringer's solution. (For the dimmer flashes the time gap between the initial flash and the jump to choline was shortened, and the traces are interrupted.) Also shown are two light-control (*LC*) records, obtained in superfusion cycles in which an intense saturating flash ($\Phi = 5 \times 10^6$) was delivered before the movement into the choline solution; one of these *LC* traces was obtained on the ninth superfusion cycle and the second on the 88th cycle. The *LC* traces are used to estimate the time course of the transient junction current that flows as a result of the difference in the solutions inside and outside the suction pipette. After the initial period of ~1 s, in choline the *LC* traces are well characterized by a single exponential decay having a time constant of 4.8 s. Finally, a dark control (*DC*) trace is shown; it is the suction current measured when the movement into choline was made entirely in darkness. The *DC* trace is the average of five cycles, but all the other traces in the figure are individual records. The inset at the lower left is a line drawing made from a videotape record of the experiment. The inset *DC–LC* plots the difference between the averaged *DC* and *LC* traces; the position of this difference trace on the time axis and its amplitude are correct, but it has been displaced arbitrarily with respect to the vertical axis. The *DC–LC* trace provides an estimate of the time course of circulating current change in the dark in choline; another method of estimating this time course is presented in connection with the data in Figs. 4 and 6.

71:22 = 3.2. Computing the ratio J_{max}/J_{dark} for each cell and averaging, we obtained the mean ratio (±SD) 3.3 (± 0.8). By instantiating Eqs. 8 and 9 twice, first for the rest (dark) condition in choline ($V = V_{rest}$, $J = J_{dark}$, $cG = cG_{dark}$), and second for the maximally activated condition ($V = V_{cG}$, $J = J_{max}$), the following expression can be derived:

$$\rho \equiv \frac{g'_{is}}{g'_{cG}} = \frac{J_{max}}{J_{dark}} - 1. \quad (11)$$

Thus, we obtained the estimate $\rho \equiv g'_{is}/g'_{cG} = 2.3$ needed for application of the model (Eq. 10). We emphasize that this estimate of ρ does not depend on the specific values of V_{is}, V_{cG}, or V_{rest} (in choline).

Aside from the reversed direction of circulating current flow, the most striking difference between the results we have obtained in choline solution containing negligible permeant cations (except for Ca^{2+}) and those previously reported for which guanidinium and lithium were used to carry the circulating current and maintain Ca^{2+}_i constant, is that in choline very much lower concentrations of Ca^{2+}_o yield approximately steady circulating currents. Fig. 6 presents data obtained from 11 rods, each exposed repeatedly to one or more choline solutions containing 0, 2.3 nM, or 7.4 nM Ca^{2+}_o. Here two kinds of data are presented: symbols represent photocurrent magnitudes, measured (as in Fig. 4) with saturating flashes given at the times when the points are plotted; the continuous traces are difference traces, *DC–LC*, as in the inset of Fig. 3. The current magnitudes are most accurately estimated with the saturating flashes (*symbols*); however, the difference traces give an additional, useful estimate of the overall time course.

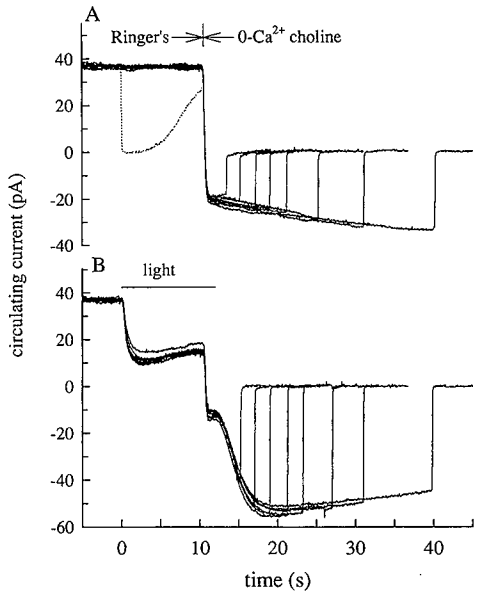

FIGURE 4. Circulating currents of a rod jumped into 0-Ca^{2+} choline in darkness (*A*) or after exposure to a step of light yielding 745 $\Phi\ s^{-1}$ (*B*). In contrast to Fig. 3, here only circulating currents have been shown, i.e., the junction current obtained from an LC record has been subtracted from all the traces before plotting. The intensity of the saturating flashes was $\Phi = 10^5$. In *A* the response to a saturating flash in Ringer's has been added (*dotted trace*) to establish the magnitude of the circulating current; the trace is truncated at the time of the jump into choline.

The data in Fig. 6 *C* establish the generality of the steady increase in circulating current in 0-Ca^{2+} choline, and the data in Fig. 6, *A* and *B*, demonstrate that this steady increase in current can be reversed by Ca^{2+}_o in the nanomolar range. In particular, the data in Fig. 6 *B* show that for $Ca^{2+}_o = 2.3$ nM, the circulating current is steady for 30 s or more. These results support the hypothesis that the increase in current in 0-Ca^{2+} choline (Figs. 4 *A* and 6 *C*) is the result of a decline in Ca^{2+}_i in the outer segment.

Further evidence that Ca^{2+}_i declines in the outer segment in 0-Ca^{2+} choline but not in choline containing 2.3 nM Ca^{2+}_o, is presented in Fig. 7. The upper panel plots four responses of a rod jumped into 2.3 nM Ca^{2+}_o; the responses, which were obtained at times ranging from 1.2 s to 29 s after the jump into choline, are nearly identical, as are the photocurrent magnitudes. The lower panel plots the responses of the same rod to flashes delivered at the same times, but now jumped into 0-Ca^{2+} choline. In contrast to those in the upper panel, the responses in the lower panel show a progressive increase in circulating current and a speeding of recovery, both of which are characteristic of a gradual lowering of Ca^{2+}_i (Fain et al., 1989).

Conclusions Regarding Ca^{2+}_i Stability in Low-calcium Choline

Our initial experimental goal was to find an experimental condition in which Ca^{2+}_i in a rod could be maintained stably at its resting level, so that the light-response kinetics could be examined without the complexity of dynamically changing Ca^{2+}_i. Two relevant conclusions emerge from consideration of the results of Figs. 4–7. The first is that while Ca^{2+}_i declines in 0-Ca^{2+} choline, the rate of decline is relatively slow, in the sense that the change in GC activity is apparently quite small over 20 s. For example, from Fig. 6 *C*, one finds that the normalized rate of increase of circulating current is ~0.02 s^{-1} over the initial 20 s. With a rate of 0.02 s^{-1}, a 40% total increase in circulating current would occur in 20 s. For a Hill coefficient of 3 (*n* in Eq. 10) and $\rho = 2.3$, this 40% increase in current corresponds to a 19% increase in *cG*. Assuming the PDE rate constant, β in Eq. 4, is unchanged, the 19% increase in *cG* corresponds to a 19% increase in guanylyl cyclase ac-

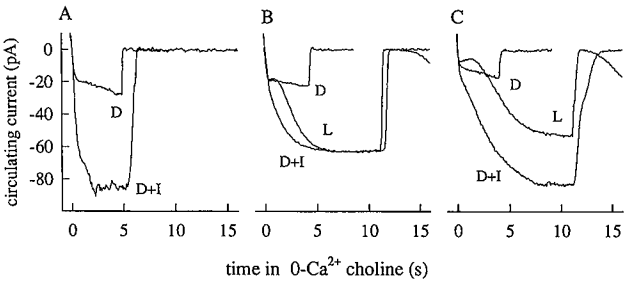

FIGURE 5. Circulating currents of three rods jumped into 0-Ca^{2+} choline in the darkness (traces labeled *D*) or after exposure in Ringer's solution to a step of light, as in Fig. 4 (traces labeled *L*). Traces labeled *I* indicate that the 0-Ca^{2+} choline contained 500 μM IBMX. The fraction of the circulating current suppressed by the light steps in Ringer's and the intensities in Φ s^{-1} were *B* (0.48, 470) and *C* (0.75, 1900). *B* and *C* show the variety of behavior exhibited when light-steps in Ringer's solution are used to decrease Ca^{2+}_i before the jump to choline.

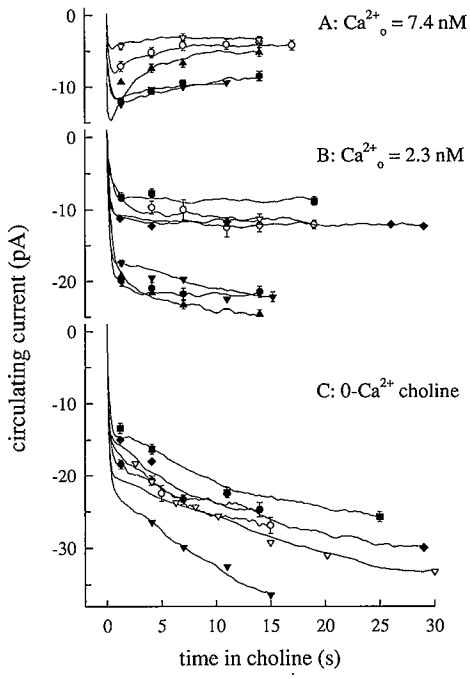

FIGURE 6. (*A–C*) Circulating currents of 11 rods jumped into choline solutions containing Ca^{2+}_o as indicated on the graphs. Symbols show the photocurrent amplitudes, measured with saturating flashes (as in Fig. 4), and noisy traces show continuous DC–LC measurements (as in the *inset* of Fig. 3). Filled symbols represent data of rods exposed to two or three levels of Ca^{2+}_o; thus, when a filled symbol is repeated in *A–C*, it refers to data of the same rod. Open symbols in different panels represent data from different rods. Error bars give ±1 SD. For display clarity, the continuous traces were digitally filtered with a Gaussian filter having f_c = 0.6 Hz (Colquhoun and Sigworth, 1983).

tivity (α in Eq. 4); for $n = 2$, the increase is cyclase activity >20 s would be 30%. We will show in the next section that such a small, steady rate of increase of cyclase activity is readily accommodated theoretically. The second conclusion is that the small increase in cyclase rate that occurs in 0-Ca^{2+} choline can be blocked by a very small amount of Ca^{2+}_o (Fig. 6 *B*, and Fig. 7), a strategy that we will adopt. A difficulty with using only the latter strategy is that the Ca^{2+}_o that must be added to eliminate the slow increase in circulating current also diminishes the current considerably (most likely by an external blocking effect on the cGMP channel), and thereby diminishes the dynamic range of the photocurrent recordings. Furthermore, since our evidence supports the hypothesis that Ca^{2+}_i changes slowly in 0-Ca^{2+} choline, it can be predicted that flash response families obtained from rods stimulated 5 s after a jump into 0-Ca^{2+} choline should exhibit approximately the same kinetics as rods jumped into choline containing 2.3 nM Ca^{2+}_o. In the next section we confirm this prediction.

Photocurrent Kinetic Analysis

Fig. 8 shows averaged responses of the rod of Fig. 3 to a series of flashes. The saturating responses in Ringer's solution (Fig. 8 *A*) and those in 0-Ca^{2+} choline (Fig. 8 *B*) follow two laws first noted by Baylor et al. (1974) in their investigation of turtle cones and by many investigators since: first, the recovery phase of the responses to saturating flashes is approximately invariant in shape when translated on the time axis; second, geometric increases in light intensity produce linear increments in the recovery time. This latter result is more clearly illustrated in Fig. 8 *C*, where we plot the time to 50% recovery as a function of the flash intensity on a semilogarithmic plot. Although confirming previous findings obtained from rods in normal Ringer's solution (Pepperberg et al., 1992), Fig. 7 also presents an entirely novel result: the slopes of the lines best fitting the recovery half-times are nearly identical: τ_c = 2.56 s and τ_c = 2.46 s per *e*-fold change in intensity for recoveries in Ringer's solution and choline, respectively.

Fig. 9 shows that the parallelism of the lines characterizing the recovery half-times in Ringer's solution and in low-Ca^{2+} choline is quite general. Here we plot the estimates of τ_c obtained from saturating responses in low-Ca^{2+} choline against τ_c determined from responses in Ringer's for 11 rods from which we obtained response families in both conditions, as in Fig. 8. In Fig. 9, open symbols represent data of rods exposed to 0-Ca^{2+} choline, whereas filled symbols represent data of rods exposed to choline containing 2.3 nM Ca^{2+}_o. The hypothesis of equality of τ_c's is represented in Fig. 9 by the positive diagonal, i.e., the unit slope line through the origin. 10 of the 12 data sets are consistent with the hypothesis, while two deviate significantly by having τ_c determined in choline reliably higher than τ_c determined in Ringer's. It is noteworthy that different rods that do not deviate from the hypothesis of equality of

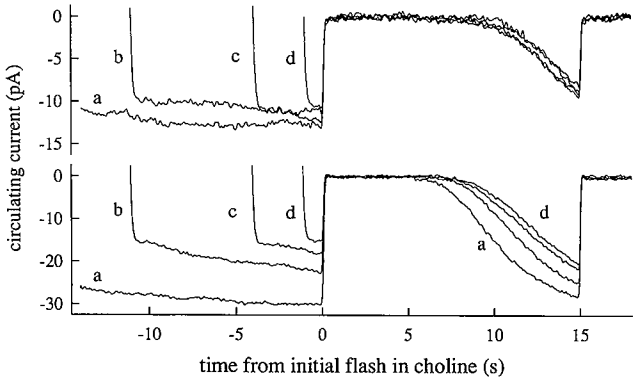

FIGURE 7. Circulating currents and photoresponses of a rod jumped into choline containing 2.3 nM $Ca^{2+}{}_o$ (*upper panel*), or 0-Ca^{2+} choline (*lower panel*). The flash (Φ = 7,100) was delivered to the rod after (*a*) 29 s, (*b*) 11 s, (*c*) 4.1 s, and (*d*) 1.25 in choline. Traces are single records, Gaussian filtered (f_c = 7 Hz). Note that the scale of the ordinate of the upper panel is twice that of the lower panel. The full time course of the circulating current changes in choline for this rod are shown in *B* and *C* of Fig. 6 (*filled diamonds*).

τ_c's do differ in a highly reliable manner from one another in their value of τ_c (Fig. 9). It is highly unlikely that these differences among rods in τ_c were caused by differences in temperature, which was always 20–22°C.

The parallelism of the recovery half-time semilog plots captured in the equality τ_c's in Fig. 9 renders the vertical shift, ΔT, between the curves interesting, for it provides a gauge of the shift of sensitivity caused by the decline in $Ca^{2+}{}_i$ from its resting level (in choline) to the very low level it reaches after saturating flashes in Ringer's solution. For example, for the data of Fig. 8 *C*, the vertical shift is ΔT = 6.5 s. By virtue of the parallelism, one can compute that in Ringer's solution a flash must be $\exp(\Delta T/\tau_c) \approx$ 13-fold more intense to produce a response having the same recovery half-time as it would have for $Ca^{2+}{}_i$ near its resting level. Table II (last column) gives sensitivity shift factors computed in this manner for all the rods studied.

Following Pepperberg et al. (1992), and intepreting τ_c as τ_{R^*}, we implemented the model described in the Theory section to describe the photoresponses in low-Ca^{2+} choline. Fig. 10 illustrates the application of the model to the responses of the rod of Fig. 8. To satisfactorily account for the data we found it necessary to augment the model with one equation in addition to those given in the theory section:

$$\alpha(t) = \alpha_{dark}(1 + k_\alpha t). \qquad (12)$$

This equation expresses the observation reported in Figs. 4 *A* and 6 *C* that there appears to be a steady increase in guanylyl cyclase activity in 0-Ca^{2+} choline. Eq. 12 may be evaluated by the degree to which the theory provides a good description of the dark control (*DC–LC*) trace in Fig. 10. To fit the responses at times longer

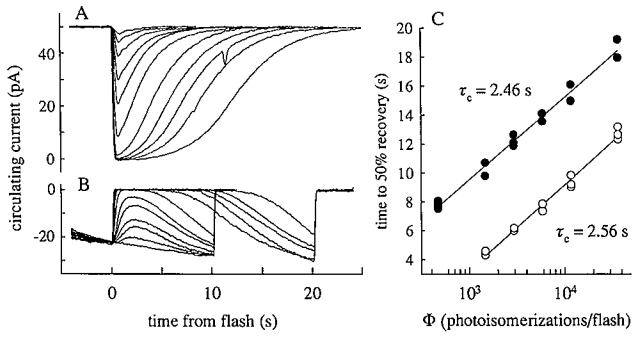

FIGURE 8. (*A*) Averaged photocurrent responses of the rod of Fig. 3 obtained in Ringer's solution to 10 ms, 500-nm flashes producing Φ = 10, 23, 45, 90, 180, 470, 1,480, 3,300, 5,900, 11,800, and 37,300 photoisomerizations. (*B*) Averaged responses obtained in 0-Ca^{2+} choline to the same series of flashes. The plotted responses to the dimmer flashes are the averages of three to five individual responses; the traces for the brighter flashes are averages of two responses. The lowermost trace is the DC–LC control and is the average from five cycles. (*C*) The times to achieve 50% recovery of the circulating current after saturating flashes are plotted as a function of flash intensity; filled symbols are for responses in 0-Ca^{2+} choline and open symbols for responses in Ringer's solution. The straight lines through the data points are fitted by the method of least squares; their slopes are given on the plot in seconds per *e*-fold change in intensity.

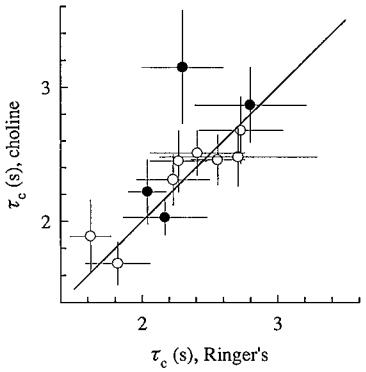

FIGURE 9. Comparison of the dominant time constant of recovery, τ_c, measured in Ringer's solution and in low-Ca^{2+} choline. Each point represents the analysis of two complete sets of saturated responses obtained from an individual cell, such as shown in Figs. 8 *C* and 11 *B*. Open symbols represent data from rods exposed to 0-Ca^{2+} choline; solid symbols represent results from rods exposed to choline containing 2.3 nM $Ca^{2+}{}_o$. For each point the values of τ_c were obtained from a least-squares regression analysis, as in Figs. 8 *C* and 11 *B*. Error bars are 95% confidence intervals for τ_c, the slope estimated from the regression analysis, computed with the standard formula (e.g., Hays, 1963, Eq. 15.22.1). The line (*positive diagonal*) represents the hypothesis that τ_c in Ringer's solution (very low $Ca^{2+}{}_i$) is identical to τ_c in low-Ca^{2+} choline ($Ca^{2+}{}_i$ approximately equal to its resting value).

than 10 s, when the rate of increase of current in 0-Ca^{2+} choline declines (Figs. 4 *A* and 6 *C*), k_α in Eq. 12 can be replaced by $k_\alpha \exp(-t/\tau_0)$, where τ_0 ranges from 15 to 25 s for different rods.

Fig. 11 *A* presents averaged photocurrents of a rod in choline having 2.3 nM $Ca^{2+}{}_o$, and theoretical curves. In Fig. 11 *B* the recovery half-time data for the saturating responses are presented, along with the best-fitting straight lines. We note a minor problem with the theoretical account of these responses. The dark-control trace (*DC–LC*) is virtually flat for 30 s (see Fig. 6, *solid diamonds*), and thus reflects balanced dark cyclase and PDE activity; thus, in terms of Eq. 12, $k_\alpha = 0$. However, in order to fit the recoveries to the more intense flashes well, k_α must be set at a nonzero value. As a compromise, we have fixed k_α at the value 0.002 s^{-1} for the entire family of theoretical traces.

Table II summarizes the application of the theoretical analysis to a population of rods from which we obtained response families including at least four saturating responses from which τ_c was estimated. In every case we found that the entire family of responses could be well described with the theory, as in Figs. 10 and 11. In two cases, we found that good reproduction of the responses to one or more intense flashes required k_α to be set to a higher value than that required to fit the dark-control trace and the dimmer flashes. In Table II, these cases (rods 5 and 10) are indicated by showing two values in the column listing k_α; the unbracketed value gives that which was used to fit most of the traces, whereas the bracketed value gives the value required to fit the responses to the most intense flashes.

DISCUSSION

Ca^{2+} Invariance of the Dominant Recovery Time Constant

When an amphibian rod is stimulated with a saturating flash, $Ca^{2+}{}_i$ declines within a few seconds from a resting value near 400 nM to a much lower value, probably 50 nM or lower (Ratto et al., 1988; Lagnado et al., 1992; Gray-Keller and Detwiler, 1994). As summarized in Fig. 9, a novel and robust finding of this investigation is that τ_c, the dominant time constant of circulating current

TABLE II

Parameters of Activation and Recovery of Salamander Rods

		Ringer's solution			Choline					Comparison	
Rod	Figs.	J_{max}	τ_c	Ca^{2+}_o	J_{max}	A	τ_{R^*}	τ_{PDE^*}	k_α	ΔT	$\exp(\Delta T/\tau_c)$
		pA	*s*	*nM*	*pA*	$s^{-2}\,\Phi^{-1}$	*s*	*s*	s^{-1}	*s*	
1	9	43 ± 0.5	1.6	0	37 ± 2	0.11	1.9	0.40	0.015	4.7	5.8
2	9	38 ± 4	2.7	0	33 ± 4	0.04	2.7	0.50	0.032	6.1	9.6
3	3, 8, 9, 10	50 ± 2	2.6	0	21 ± 2	0.045	2.5	0.47	0.016	6.5	12.8
4	6 *C*, 9	47 ± 3	1.8	0	23 ± 1	0.048	1.7	0.40	0.032	5.5	23.2
5	9	48 ± 2	2.7	0	30 ± 2	0.044	2.5	0.30	0.005 (0.024)	5.5	9.3
6	9	39 ± 0.5	2.3	0	19 ± 1	0.065	2.4	0.50	0.026	6.8	14.4
7	9	41 ± 0.5	2.4	0	18 ± 1	0.060	2.5	0.50	0.030	5.6	9.8
8a	6 *C*, 9	38 ± 1	2.2	0	16 ± 2	0.085	2.3	0.40	0.028	5.0	9.2
9	6 *B*, 9	24 ± 2*	2.8	2.3	12 ± 1	0.060	2.9	0.45	0.007	8.5	19.7
10	6 *B*, 9	37 ± 1	2.3	2.3	13 ± 1	0.055	2.8	0.45	0.001 (0.024)	7.9	22.1
8b	6 *B*, 9	43 ± 2	2.2	2.3	12 ± 1	0.08	2.0	0.40	0.006	5.6	14.4
11	6 *B*, 6 *C*, 7, 9, 11	31 ± 2*	2.0	2.3	12 ± 0.4	0.047	2.2	0.35	0.002	6.5	18.0
	Mean ± SD	41 ± 7	2.30 ± 0.37		—	0.06 ± 0.02	2.36 ± 0.37	0.43 ± 0.06	—	6.2 ± 1.1	14.0 ± 5.6

Column 1 identifies the rod; rod number 8 was recorded from under three conditions, Ringer's solution and two different levels of $Ca^{2+}{}_o$. Column 2 gives figures in which data from the rod appear. Column 3 gives the maximum circulating current in Ringer's solution; these values are somewhat diminished from the values that would be obtained were the outer segment not positioned completely outside the suction electrode (see Methods). The values denoted with an asterisk * were obtained in experiments in which the outer segment was placed more than 5 μm outside the pipette constriction in an effort to eliminate any influence of the Ringer's solution inside the suction pipette. Column 4 gives the value of τ_c estimated from families of saturating flashes in Ringer's solution, as in Figs. 8 *C* and 11 *B*. Column 5 gives the value of $Ca^{2+}{}_o$ for the choline test solution. Column 6 gives the maximum circulating current recorded in choline, measured 5 s after the jump for rods in 0-Ca^{2+} choline, and 5 or 12 s after the jump for $Ca^{2+}{}_o$ = 2.3 nM. Column 7 gives the estimate of the amplification constant (see Table I). Column 8 gives τ_c estimated from families of saturating flashes in choline, which is identified in the model as a first-order time constant for inactivation of R*. Column 9 gives the estimate of the time constant for simultaneous inactivation of G* and PDE*. Column 10 gives the apparent rate of activation of GC in choline (Eq. 11), obtained from fitting a response family, including and especially, the dark control trace; the two bracketed entries indicate instances in which a higher value of the parameter had to be used to fit one or more of the responses to more intense flashes. Column 11 gives the vertical shift in seconds between parallel lines fit to the recovery half-time plots (e.g., Figs. 8 *C*, 11 *B*); column 12 converts the vertical shift into an effective change in sensitivity, as described in the text.

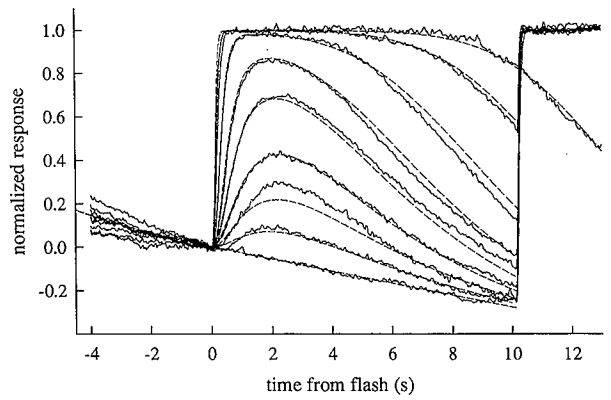

FIGURE 10. Application of the theoretical model to photocurrent responses of a dark-adapted rod in 0-Ca^{2+} choline. The noisy traces are the normalized records from Fig. 8 *B*; the dashed lines give calculations done with the model. The magnitude of the maximal photocurrent 5 s after the jump into choline was 20.9 ± 2.1 pA (26 responses). The values of the model parameters are provided in Table II. To optimize the fitting, τ_{R^*} was set equal to τ_c, obtained from regression analysis of the choline data in Fig. 8 *C*; τ_{PDE^*} was varied to find the best fit of the model to the traces.

recovery after a saturating flash, has essentially the same value in Ringer's solution as in low-Ca^{2+} choline solution. This finding implies that the biochemistry underlying τ_c has little or no sensitivity to changes in $Ca^{2+}{}_i$ in the physiologic range. In particular, if, as hypothesized by Pepperberg et al. (1992), τ_c can be ascribed to

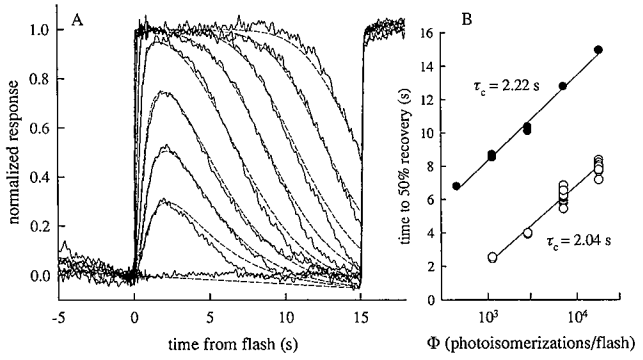

FIGURE 11. (*A*) Averaged photocurrent responses of a rod in choline containing 2.3 nM Ca^{2+} to 20 μs nm flashes producing Φ = 45, 90, 180, 450, 1,130, 2,900, 7,100, and 19,500 photoisomerizations (*noisy traces*) and application of the theoretical model (*dashed lines*). The values of the parameters and other characteristics of the rod are given in Table II; τ_{R^*} was set equal to τ_c, obtained from regression analysis of the choline data shown in *B*. The magnitude of the maximal photocurrent 12 s after the jump into choline was 11.8 ± 0.4 pA (seven responses). The initial flashes were delivered at 12 s after the jump into choline; the time course of circulating current in the dark for this rod for 30 s is shown in Fig. 6 *B* in the trace associated with the filled diamonds. (*B*) Recovery half-times of the rod to flashes delivered in normal Ringer's solution (*open symbols*) and in choline solution (*filled symbols*).

the inactivation of R*, then the hypothesis that the lifetime of R* is regulated by changes in $Ca^{2+}{}_i$ is falsified. Others, investigating the role of $Ca^{2+}{}_i$ in regulating response sensitivity, have proposed that the lifetime of R* might be calcium dependent (Torre et al., 1986; Kawamura, 1993; Lagnado and Baylor, 1994).

Kinetic Sufficiency of Two First-order Inactivations in the First Three Cascade Steps

Our application of the model of the G-protein cascade (Figs. 10 and 11, and Table II) demonstrates that when $Ca^{2+}{}_i$ is maintained near its resting level, the recovery phase of the first three steps of the cascade can be adequately characterized by two first-order decay steps: a dominant decay step with time constant of 1.6–2.8 s, and a faster decay with a time constant of about 0.3–0.5 s. By incorporating these time constants into the successful activation model of Lamb and Pugh (1992), we have shown that these decay steps can be formally ascribed to the inactivation of the two enzymatic amplifiers, R* and PDE*. In previous investigations, it has been proposed that three different time constants might be needed to characterize the inactivation of the first three steps of the cascade (Tamura et al., 1991).

A strong caution needs to be voiced regarding the identity of the mechanisms underlying the two first-order inactivations in the model. In keeping with the hypothesis of Pepperberg et al. (1992), we identified the dominant time constant, τ_c with a hypothetical first-order decline of the enzymatic activity of R*. Unfortunately, the ability of the model to provide a good account of the responses in clamped $Ca^{2+}{}_i$ (Figs. 10 and 11) provides no support for the identification. This follows, because over the intensity range of our experiments, Eq. 4 is linear in Φ and the two time constants, τ_{R^*} and τ_{PDE^*}, are formally interchangeable, as is necessary in any cascaded linear system. Identification of the mechanism underlying τ_c will require kinetic and pharmacologic analysis of recoveries to flashes of higher intensities than used here (Pepperberg et al., 1992).

Estimate of the Magnitude of the Sensitivity Changes Caused by Decline in $Ca^{2+}{}_i$

Whereas the dominant time constant of recovery, τ_c, remains largely unaffected by the decline in $Ca^{2+}{}_i$ that occurs during the response to saturating flashes in Ringer's solution, the overall time course of recovery clearly is sped up. Because of the parallelism of the recovery half-time semilog plots (Figs. 8 *B*, 9, and 11 *B*), $\exp(\Delta T/\tau_c)$ provides a measure of the overall effect on apparent sensitivity of the biochemical mechanisms that respond to the decline in $Ca^{2+}{}_i$. The average overall effect was 14-fold, but in many cases it was 20-fold or more (Table II, last column). A 14- to 20-fold sensitivity shift is equivalent to all but the compressive gain con-

trol in salamander rod light adaptation (Matthews et al., 1988; Nakatani and Yau, 1988). For example, Matthews et al. (1988) found that steady lights that suppress 90% of the circulating current produce a 160-fold decline in dim-flash sensitivity, when sensitivity is defined in the absolute units of pA/Φ for dim flashes. Since 10-fold of this overall sensitivity reduction is the result of the compressive effect of the 90% decrease in current, the residual factor of sensitivity change not accounted for is 16. This is essentially the same factor we found to decrease the effectiveness of saturating flashes in Ringer's solution.

Calcium Balance in Low-Na^+ Solutions

In previous investigations in which the maintenance of constant $Ca^{2+}{}_i$ was effected by removing external Na^+ and most Ca^{2+}, guanidinium or Li^+ was substituted for Na^+ as the current carrier through the cGMP-activated conductance, and concentrations of $Ca^{2+}{}_o$ of 1–3 μM were used to maintain $Ca^{2+}{}_i$ near rest (Fain et al., 1989). Assuming that $Ca^{2+}{}_i|_{rest}$ is ~ 400 nM (see above), and that rods in guanidium have $V_{rest} \approx -30$ mV, the $Ca^{2+}{}_o$ required for circulating current stability in guanidium is ~25- to 75-fold higher than the concentration predicted by the Nernst equation, were Ca^{2+} in equilibrium. In contrast to the previous investigations, our evidence shows $Ca^{2+}{}_i$ to be stable in choline solutions containing no other permeant cations except $Ca^{2+}{}_o$ estimated to be 2.3 nM (Fig. 6), a concentration ~1,000-fold lower than those of the earlier experiments. If $V_{rest} \approx -67$ mV (J_{cG} = 12 pA; Table II; cf. Fig. 1 *B*), then the $Ca^{2+}{}_o$ required for circulating current stability, 2.3 nM, is very near the predicted equilibrium concentration, 2.0 nM. These calculations suggest that there is considerable residual Ca^{2+} pumping in the dark steady state in the earlier guanidium/lithium experiments, and little in the choline experiments presented here.

We thank Dr. T. D. Lamb for much helpful criticism.

This work was supported by National Institutes of Health grant EY-02660.

Original version received 15 May 1995 and accepted version received 13 September 1995.

REFERENCES

Angleson, J. K., and T. G. Wensel. 1994. Enhancement of rod outer segment GTPase accelerating protein activity by the inhibitory subunit of cGMP phosphodiesterase. *J. Biol. Chem.* 269:16290–16296.

Arshavsky, V. Y., and M. D. Bownds. 1992. Regulation of deactivation of photoreceptor G protein by its target enzyme and cGMP. *Nature (Lond.).* 357:416–417.

Arshavsky, V. Y., C. L. Dumke, and M. D. Bownds. 1992. Non-catalytic cGMP binding sites of amphibian rod cGMP phosphodiesterase control interaction with its inhibitory γ-subunits. A putative regulatory mechanism of the rod photoresponse. *J. Biol. Chem.*. 267:24501–24507.

Arshavsky, V. Y., C. L. Dumke, Y. Zhu, N. O. Artemyev, N. P. Skiba, H. E. Hamm, and M. D. Bownds. 1994. Regulation of transducin GTPase activity in bovine rod outer segments. *J. Biol. Chem.* 269: 19882–19887.

Bader, D. R., P. R. MacLeish, and E. A. Schwartz. 1979. A voltage-clamp study of the light response in solitary rods of the tiger salamander. *J. Physiol. (Lond.).* 296:1–26.

Baylor, D. A., A. L. Hodgkin, and T. D. Lamb. 1974. The electrical response of turtle cones to flashes and steps of light. *J. Physiol. (Lond.).* 242:685–727.

Baylor, D. A., and B. J. Nunn. 1986. Electrical properties of the light-sensitive conductance of rods of the salamander *Ambystoma tigrinum*. *J. Physiol. (Lond.).* 371:115–145.

Bennett, N., and A. Sitaramayya. 1988. Inactivation of photoexcited rhodopsin in retinal rods: the roles of rhodopsin kinase and 48-dDa protein (Arrestin). *Biochemistry.* 27:1710–1715.

Breton, M. E., A. W. Schueller, T. D. Lamb, and E. N. Pugh, Jr. 1994. Analysis of ERG α-wave amplification and kinetics in terms of the G-protein cascade of phototransduction. *Invest. Ophthalmol. Vis. Sci.* 35:295–309.

Chen, C.-K., J. Inglese, R. J. Lefkowitz, and J. B. Hurley. 1994. $Ca^{2+}{}_i$-dependent interaction of recoverin with rhodopsin kinase. *J. Biol. Chem.* 270:1–7.

Cobbs, W. H., and E. N. Pugh, Jr. 1987. Kinetics and components of the flash photocurrent of isolated retinal rods of the larval salamander *Ambystona tigrinum*. *J. Physiol. (Lond.).* 394:529–572.

Colquhoun, D., and F. J. Sigworth. 1983. Fitting and statistical analysis of single-channel records. *In* Single-Channel Recording. B. Sakmann and E. Neher, editors. Plenum Publishing Corp., New York.

Dumke, C. L., V. Y. Arshavsky, P. D. Calvert, M. D. Bownds, and E. N. Pugh, Jr. 1994. Rod outer segment structure influences the apparent kinetic parameters of cyclic GMP phosphodiesterase. *J. Gen. Physiol.* 103:1071–1098.

Durham, A. C. H. 1983. A survey of readily available chelators for buffering calcium ion concentrations in physiological solutions. *Cell Calcium.* 4:33–46.

Fain, G. L., T. D. Lamb, H. R. Matthews, and R. L. W. Murphy. 1989. Cytoplasmic calcium as the messenger for light adaptation in salamander rods. *J. Physiol. (Lond.).* 416:215–243.

Gorczya, W. A., M. P. Gray-Keller, P. B. Detwiler, and K. Palczewski. 1994. Purification and physiological evaluation of a guanylate cyclase activating protein from retinal rods. *Proc. Natl. Acad. Sci. USA.* 91:4014–4018.

Gray-Keller, M. P., and P. B. Detwiler. 1994. The calcium feedback signal in the phototransduction cascade of vertebrate rods. *Neuron.* 13:849–861.

Hagins, W. A., R. D. Penn, and S. Yoshikami. 1970. Dark current and photocurrent in retinal rods. *Biophys. J.* 10:380–412.

Hays, W. L. 1963. Statistics. Holt, Rinehart and Winston, New York.

Hodgkin, A. L., and B. J. Nunn. 1988. Control of light-sensitive current in salamander rods. *J. Physiol. (Lond.).* 403:439–471.

Hodgkin, A. L., P. A. McNaughton, B. J. Nunn, and K.-W. Yau. 1984. Effect of ions on retinal rods from *Bufo marinus*. *J. Physiol. (Lond.).* 350:649–680.

Hodgkin, A. L., P. A. McNaughton, and B. J. Nunn. 1985. The ionic selectivity and calcium dependence of the light-sensitive pathway in toad rods. *J. Physiol. (Lond.).* 358:447–468.

Hodgkin, A. L., P. A. McNaughton, and B. J. Nunn. 1987. Measurement of sodium-calcium exchange in salamander rods. *J. Physiol. (Lond.).* 391:347–370.

Hofmann, K. P., and M. Heck. 1995. Light-induced protein-protein interactions on the rod photoreceptor disc membrane. *In* Biomembranes II. Lee, editor. JAI Press.

Hood, D. C., and D. G. Birch. 1994. Rod phototransduction in retinitis pigmentosa: estimation and interpretation of parameters derived from the rod α-wave. *Invest. Ophthalmol. Vis. Sci.* 35:2948–2961.

Kahlert, M., D. R. Pepperberg, and K. P. Hofmann. 1990. Effect of bleached rhodopsin on signal amplification in rod visual receptors. *Nature (Lond.).* 345:537–539.

Karpen, J. W., A. L. Zimmerman, L. Stryer, and D. A. Baylor. 1988. Gating kinetics of the cyclic GMP-activated channel of retinal rods: flash photolysis and voltage clamp studies. *Proc. Natl. Acad. Sci. USA.* 85:1287–1291.

Kawamura, S. 1993. Rhodopsin phosphorylation as a mechanism of cyclic GMP phosphodiesterase regulation by S-modulin. *Nature (Lond.).* 362:855–857.

Klenchin, V. A., P. D. Calvert, and M. D. Bownds. 1995. Inhibition of rhodopsin kinase by recoverin: evidence for a negative feedback system in phototransduction. *J. Biol. Chem.* 270:16147–16152.

Kraft, T. W., D. M. Schneeweis, and J. L. Schnapf. 1993. Visual transduction in human rod photoreceptors. *J. Physiol. (Lond.).* 464:747–765.

Lagnado, L., and D. A. Baylor. 1994. Calcium controls light-triggered formation of catalytically active rhodopsin. *Nature (Lond.).* 367:273–277.

Lagnado, L., L. Cervetto, and P. A. McNaughton. 1992. Calcium homeostasis in the outer segments of retinal rods from the tiger salamander. *J. Physiol.* 455:111–142.

Lamb, T. D. 1994. Stochastic simulation of activation in the G-protein cascade of phototransduction. *Biophys. J.* 67:1439–1454.

Lamb, T. D., and H. R. Matthews. 1988. Incorporation of analogues of GTP and GDP into rod photoreceptors isolated from the tiger salamander. *J. Physiol. (Lond.).* 407:463–487.

Lamb, T. D., and Pugh, E. N., Jr. 1992. A quantitative account of the activation steps involved in phototransduction in amphibian photoreceptors. *J. Physiol. (Lond.).* 449:719–758.

Matthews, H. R. 1995. Effects of lowered cytoplasmic calcium concentration and light on the responses of salamander rod photoreceptors. *J. Physiol. (Lond.)* 484:267–286.

Matthews, H. R., R. L. W. Murphy, G. L. Fain, and T. D. Lamb. 1988. Photoreceptor light adaptation is mediated by cytoplasmic calcium concentration. *Nature (Lond.).* 334:67–69.

Miller, J. L., and J. I. Korenbrot. 1994. Differences in calcium homeostasis between retinal rod and cone photoreceptors revealed by the effects of voltage on the cGMP-gated conductance in intact cells. *J. Gen. Physiol.* 104:909–940.

Nakatani, K., and K.-W. Yau. 1988. Calcium and light adaptation in retinal rods and cones. *Nature (Lond.).* 334:69–71.

Nakatani, K., and K.-W. Yau. 1989. Sodium-dependent calcium extrusion and sensitivity regulation in retinal cones of the salamander. *J. Physiol. (Lond.).* 409:525–548.

Palczweski, K., I. Subbaraya, W. A. Gorczyca, B. S. Helekar, C. C. Ruiz, H. Phguro, J. Huang, X. Zhao, J. W. Crabb, R. S. Johnson, K. A. Walsh, M. P. Gray-Keller, P. B. Detwiler, and W. Baehr. 1994. Molecular cloning and characterization of retinal photoreceptor guanylyl cyclase-activating protein. *Neuron.* 13:1–20.

Pepperberg, D. R., M. C. Cornwall, M. Kahlert, K. P. Hofmann, J. Jin, G. J. Jones, and H. Ripps. 1992. Light-dependent delay in the falling phase of the retinal rod photoresponse. *Vis. Neurosci.* 8:9–18.

Pepperberg, D. R., M. Kahlert, A. Krause, and K. P. Hofmann. 1988. Photic modulation of a highly sensitive, near-infrared light-scattering signal recorded from intact retinal photoreceptors. *Proc. Natl. Acad. Sci. USA.* 85:5531–5535.

Pugh, E. N., Jr., and T. D. Lamb. 1993. Amplification and kinetics of the activation steps in phototransduction. *Biochim. Biophys. Acta.* 1141:111–149.

Ratto, G. M., R. Payne, W. G. Owen, and R. Y. Tsien. 1988. The concentration of cytosolic free calcium in vertebrate outer segments measured with fura-2. *J. Neurosci.* 8:3240–3246.

Sitaramayya, A., and P. A. Liebman. 1983. Mechanism of ATP quench of phosphodiesterase activation in rod disc membranes. *J. Biol. Chem.* 258:1205–1209.

Tamura, T., K. Nakatani, and K.-W. Yau. 1991. Calcium feedback and sensitivity regulation in primate rods. *J. Gen. Physiol.* 98:95–130.

Torre, V., H. R. Matthews, and T. D. Lamb. 1986. Role of calcium in regulating the cyclic nucleotide cascade of phototransduction in retinal rods. *Proc. Natl. Acad. Sci. USA.* 83:7109–7113.

Tsien, R. Y. 1983. Intracellular measurements of ion activities. *Annu. Rev. Biophys. Bioeng.* 12:91–116.

Wilden, U., S. W. Hall, and H. Kuhn. 1986. Phosphodiesterase activation by photoexcited rhodopsin is quenched when rhodopsin is phosphorylated and binds the intrinsic 48 KDa protein of rod outer segments. *Proc. Natl. Acad. Sci. USA.* 83:1174–1178.

Yau, K.-W., and D. A. Baylor. 1989. Cyclic GMP-activated conductance of retinal photoreceptor cells. *Annu. Rev. Neurosci.* 12:289–327.